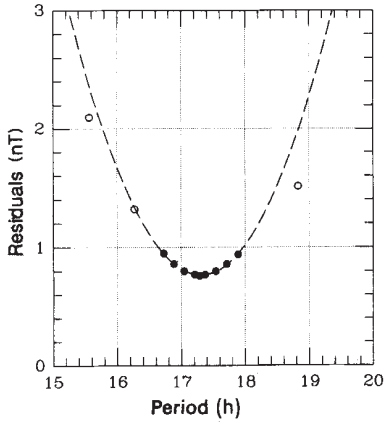

Fig. 3 Root-mean-square residual error between the best-fitting magnetic field model and the observations, as a function of assumed rotation period. The minimum r.m.s. error was obtained for a rotation period of 17.29 h. The parabolic least-squares line, shown by the dashed curve, is fit to the filled points.

tainty in the period measurement of ±0.003 h. The final determination from the radioastronomy data is, therefore, 17.239 ± 0.009 h.

The magnetic field data provide a direct measure of the rotation period of the planet's interior, where the field is generated. The data used in this study spanned the interval from 15:00 to 21:00 (spacecraft time) on 24 January 1986. During this time Voyager 2 traversed the innermost magnetosphere, passing from a radial distance of 8 R_U (the planet radius R_U = 25,600 km) at 40° S latitude, through closest approach (4.2 R_U), to a radial distance of 8 R_U at 78° N latitude. The maximum observed magnetic field, measured just before closest approach, was 413 nT. Without accurate knowledge of the planet's rotation period, the location of the spacecraft in the reference frame rotating with Uranus is unknown, making global magnetic field determinations difficult. In order to determine the rotation period, spherical harmonic analyses were performed with the rotation period treated as a free parameter. For each assumed period, ranging from 15.5 to 18.8 h, the best-fitting I2E1 (dipole plus quadrupole internal field plus uniform external field) model was found.

Figure 3 shows the root-mean-square (r.m.s.) residual between the best-fitting models and the observations as a function of assumed period. The best fit was obtained for a rotation period of 17.29 h, for which the r.m.s. error was 0.76 nT. We believe that this residual error is largely due to that part of the external fields (for example, fields due to the magnetopause and magnetotail currents) not well approximated by a uniform field. Figure 3 also shows a parabolic least-squares fit to the points having r.m.s. error <1 nT; the uncertainty in the parabola coefficients yields an uncertainty of ±0.05 h in the rotation period.

The I2E1 model is the simplest spherical harmonic model for which an acceptable fit to the observations is obtained. Centred dipole models fit poorly (r.m.s. error >7.8 nT) for all assumed rotation periods. An offset, tilted dipole representation of the field, presented in ref. 8, has an associated r.m.s. error of 2.4 nT. More complex (for example, octupole) models can be considered only in part using generalized inverse methods[10], because of the limited observations. An examination of the impact of increasing model complexity on the deduced rotation rate suggests an uncertainty several times that obtained assuming an I2E1 model, or ~ ± 0.2 h. The best direct estimate of the rotation period is then 17.29 ± 0.2 h.

The two period determinations made here are entirely independent and self-consistent. Combining the two periods yields a weighted mean value of P = 17.24 ± 0.01 h. As no further spacecraft observations of Uranus are planned at this time, we believe that this value is not likely to be improved upon in the foreseeable future.

The 17.24-h rotation period has important consequences for studies of atmospheric dynamics[12] and the internal structure and composition of Uranus. Inferences regarding the internal structure can be drawn from the relationship between the observed planetary oblateness, rotation period and gravitational moment (J_2). The latter two are now known with great precision, constraining plausible models of the interior. Several 2- and 3-layer models, incorporating a 'rock' core, 'ice' mantle and gaseous outer envelope, have been considered[13,14] for Uranus. A model (U4, ref. 14) containing a rocky core of ~6.6 Earth masses ($M_\oplus$) and an outer envelope with ~3.7 $M_\oplus$ H_2–H gas and 4.4 $M_\oplus$ ice is most consistent with the rotation period reported here.

We thank our colleagues on the Voyager magnetometer investigation, led by principal investigator N. Ness; our colleagues on the Voyager planetary radioastronomy investigation, led by J. Warwick; and the data processing and display staff of the Laboratory for Extraterrestrial Physics, GSFC, under the direction of W. Mish, for support during the intensive Uranus encounter.

Received 23 April; accepted 16 May 1986.

1. Brown, R. A., Goody, R. *Astrophys. J.* **235**, 1066–1070 (1980).
2. Trauger, J. T., Roessler, F. L. & Munch, G. *Astrophys. J.* **219**, 1070–1083 (1978).
3. Trafton, L. *Icarus* **32**, 402–412 (1977).
4. Munch, G. & Hippelein, H. *Astr. Astrophys.* **81**, 189–197 (1979).
5. Elliot, J. L. *et al. Astr. J.* **86**, 444–455 (1981).
6. Goody, R. in *Uranus and the Outer Planets* (ed. Hunt, G.) (Cambridge University Press, 1982).
7. Warwick, J. W. *et al. Science* (in the press).
8. Ness, N. F. *et al. Science* (in the press).
9. Desch, M. D. & Kaiser, M. L. *Geophys. Res. Lett.* **8**, 253–256 (1981).
10. Connerney, J. E. P. *J. geophys. Res.* **86**, 7679–7693 (1981).
11. Stone, P. H. *Icarus* **24**, 292–298 (1975).
12. Smith, B. *et al. Science* (in the press).
13. Hubbard, W. B. & MacFarlane, J. *J. geophys. Res.* **85**, 225–234 (1980).
14. Podolak, M. & Reynolds, R. T. *Icarus* **46**, 40–50 (1981).

Detection of stratospheric HNO_3 and NO_2 response to short-term solar ultraviolet variability

G. M. Keating*, J. Nicholson III†, G. Brasseur‡, A. De Rudder‡, U. Schmailzl§ & M. Pitts‖

* Atmospheric Sciences Division, NASA Langley Research Center, Hampton, Virginia 23665-5225, USA
† Vigyan Research Associates, Hampton, Virginia 23666, USA
‡ Institut d'Aéronomie Spatiale, 1180 Brussels, Belgium
§ Max Planck Institute for Chemistry, 6500 Mainz, FRG
‖ SASC Technologies, Hampton, Virginia 23666, USA

Variations in the solar ultraviolet irradiance with a period equal to or approximately one-half of the rotation period of the Sun (27 days) are currently observed by satellite monitoring. These variations have typical peak-to-peak amplitudes of ~3% between 170 and 208 nm and <1.5% at longer wavelengths. Detection of the response of stratospheric species to solar ultraviolet variability is crucial for understanding the photochemical behaviour of the middle atmosphere. Understanding the natural variations of the stratosphere is also a prerequisite for isolating possible anthropogenic effects; up to now most work has concerned stratospheric ozone[1–8]. Recent analysis[5] of measurements by the Nimbus 7 satellite's LIMS (limb infrared monitor of the stratosphere) and SBUV (solar backscatter ultraviolet) experiments has established very high correlations between ozone mixing ratios (detrended and corrected for temperature effects) and short-term variations in 205-nm solar radiation. A similar approach is used here to detect

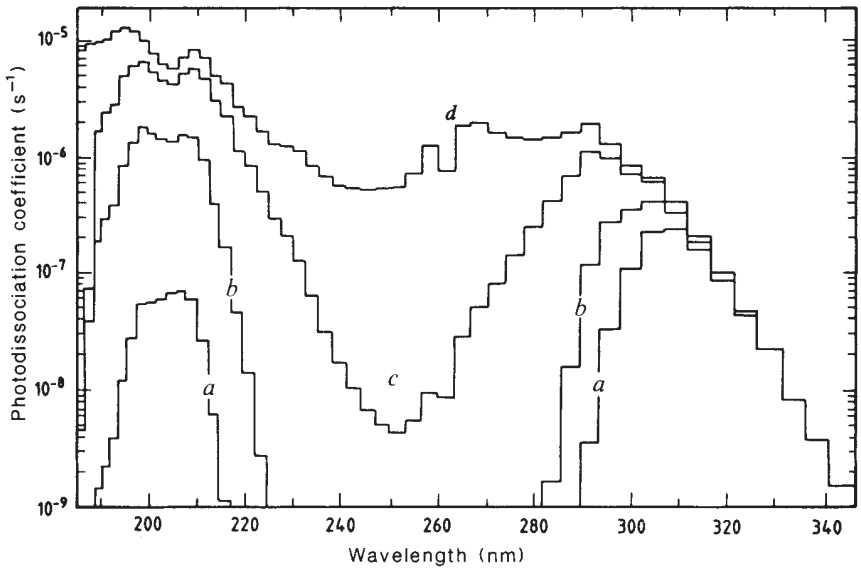

Fig. 1 Spectral distribution between 185 and 345 nm of the photodissociation coefficient of nitric acid for selected altitudes: *a*, 20 km; *b*, 30 km; *c*, 40 km; *d*, top of the atmosphere. The calculation assumes an overhead Sun (from ref. 16).

a relation between LIMS measurements of HNO_3[9,10] and NO_2[11] and the SBUV measurements of short-term variations in 205-nm radiation[12]. Observations show that the response of HNO_3 is much stronger than, but in the opposite sense to the ozone response, and that the NO_2 response is in the opposite sense to the HNO_3 response. This is the first detection of such a response for species other than ozone. Model calculations are in fair agreement with observed short-term variations and predict large variations in HNO_3 over the 11-yr solar cycle.

Nitrous oxide (N_2O) is the major source of odd nitrogen ($N + NO + NO_2 + NO_3 + 2N_2O_5 + HNO_3 + HO_2 + HO_2NO_2 + ClONO_2$) in the stratosphere. It is formed in the soil by bacterial action and transported into the middle atmosphere, where it is destroyed by photodissociation or by reaction with the electronically excited oxygen atom $O(^1D)$. Nitric oxide (NO), which is produced by the reaction of N_2O with $O(^1D)$, is converted to nitrogen dioxide (NO_2) essentially through reaction with ozone, but also by reaction with ClO, HO_2 or CH_3O_2. The NO_2 molecule reacts rapidly during the day to form NO either by reaction with O or by photolysis. During the night a significant amount of NO_2 reacts with O_3 to produce NO_3, which, in turn, is converted into N_2O_5 by reaction with NO_2. After sunrise the N_2O_5 concentration decreases continuously as solar ultraviolet radiation (primarily above 300 nm) photodissociates the molecule, replenishing NO_2. The behaviour of NO_2 is also affected by chlorine compounds, as $ClONO_2$ is formed by the three-body reaction of ClO and NO_2. The $ClONO_2$ is partly destroyed during the day by photodissociation or reaction with O or OH. Nitric acid is formed by the three-body reaction

$$NO_2 + OH \xrightarrow{M} HNO_3 \quad (1)$$

The HNO_3 molecule is relatively stable in the lower stratosphere and is therefore subject to a variety of transport processes leading, for example, to large mixing ratios at high latitudes. The loss processes for HNO_3 are

$$HNO_3 + h\nu \rightarrow OH + NO_2 \quad (2)$$

and

$$HNO_3 + OH \rightarrow NO_3 + H_2O \quad (3)$$

The sensitivity of HNO_3 to change in the solar ultraviolet output is predicted by a one-dimensional time-dependent chemical-radiative model[13,14]. The short-term spectral variability[5] of the solar irradiance is applied in the model in accord with the solar data of Heath *et al.*[12]. The average solar ultraviolet irradiances adopted in the model are based on ref. 15, and we assume a sinusoidal variation of the solar ultraviolet output.

At 10 mbar, the model predicts a reduction of 0.4% in HNO_3 for a 1% increase in solar radiation at 205 nm, with a response time of less than 1 day. This strong response to short-term solar ultraviolet variations can be understood by referring to Fig. 1 (see ref. 16), in which the photodissociation frequency of HNO_3 at different altitudes is shown as a function of wavelength for overhead Sun conditions. The decrease of photodissociation with decreasing altitude for wavelengths centred on 250 nm is due to increasing ozone absorption. The sharp decrease below 200 nm is due to absorption in the molecular oxygen Schuman-Runge bands. The net effect of solar absorption by stratospheric O_3 and O_2 results in an enhancement of the effects of solar variability near 200 nm on the photodissociation of HNO_3.

The detection of the HNO_3 response to ultraviolet variations can be expected only in regions of the atmosphere where the chemical lifetime is short compared with the transport lifetime, and significantly shorter than the period of the solar oscillation. A calculation based on the model of Crutzen and Schmailzl[17] shows that the chemical lifetime of HNO_3 increases with decreasing altitude and, at a given level, increases with latitude, particularly in winter At 10 mbar near equinox, for example, the HNO_3 lifetime is enhanced by 40% going from 0 to 40° latitude, while at 20 mbar it is enhanced by 60% over the same latitudinal range. In winter, the variation of the lifetime at a given altitude is larger than in other seasons. At 10 mbar, for example, the lifetime increases by more than 300% between 0 and 40° latitude. Therefore, data from near the winter solstice and high-latitude data (latitudes > 40°) were removed from the LIMS data set. Moreover, the width of the latitudinal region about the Equator from which data were used was decreased at lower altitudes (±40° at 10 mbar and ±20° at 20 mbar), to reduce dynamical effects. By this method, the data examined were limited to those from atmospheric regions where the photochemical lifetime of HNO_3 is calculated to be less than 2 days.

Finally, to remove any possible bias, the measurements were detrended relative to a running mean, averaged over a period slightly longer than the solar oscillation period characteristic of the interval investigated (similar to the approach used for the ozone data by Keating *et al.*[5]). No significant HNO_3–temperature relation was predicted or observed at this level, so no correction was made. At 10 mbar, Fig. 2 shows the resulting relation between the ultraviolet ratio $(I_{205} - \bar{I}_{205})/\bar{I}_{205}$ and the dayside HNO_3 ratio $(HNO_3 - \overline{HNO})/\overline{HNO}_3$, where I_{205} is the 5-day running mean of the 205-nm solar radiation, $\bar{I}_{205}$ is the 19-day running mean of I_{205}, HNO_3 is the 5-day running mean of the nitric acid volume mixing ratio averaged zonally and averaged between +40° and −40° latitude, and $\overline{HNO}_3$ is the

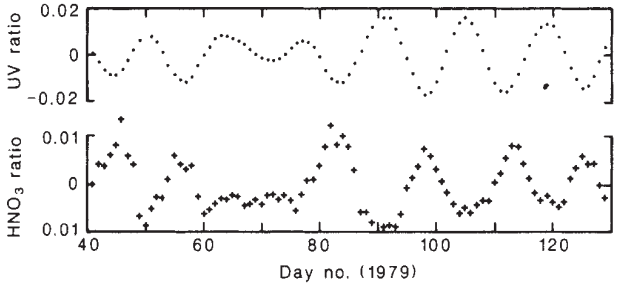

Fig. 2 Relation between dayside nitric acid ratio $[(HNO_3 - \overline{HNO_3})/\overline{HNO_3}]$ at 10 mbar (+) and 205-nm solar irradiance (UV) ratio $[(I_{205} - \bar{I}_{205})/\bar{I}_{205}]$ (●) between days 40 and 130 of 1979. The correlation coefficient between the two parameters is $r = -0.78$.

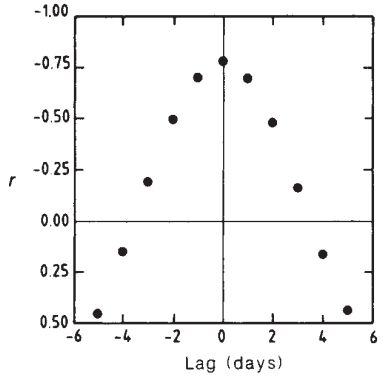

Fig. 3 Correlation coefficient between the nitric acid ratios and the 205-nm solar irradiance ratios in Fig. 2 for different time lags between these two quantities.

19-day running mean of HNO_3. Clearly, HNO_3 is negatively correlated with the approximate 13.5-day solar ultraviolet oscillation. The correlation coefficient between the two parameters shown in Fig. 2 is −0.78. This correlation with the 205-nm solar irradiance is significantly higher than the correlation (−0.38) with the emission from the Sun at 10.7 cm (the classical 10.7-cm solar index). This is to be expected because, as indicated previously, the 205-nm radiation is very efficient in photodissociating HNO_3 throughout the stratosphere. The regression coefficient (sensitivity) for the 10-mbar dayside HNO ratio against the ultraviolet ratio is -0.44 ± 0.07 (2σ uncertainty). In order to determine the lag time between the solar variability and the nitric acid response, the correlation coefficient between the two parameters was determined as a function of positive and negative lag (days). The resulting relationship is shown in Fig. 3: the maximum correlation occurs for a lag of 0 ± 1 days.

The 0.44% reduction in HNO_3 at 10 mbar can be compared with the variation of ozone at the same level. At low latitudes, the ozone response is calculated to be an increase of 0.17% for a 1% increase in 205-nm radiation, with a response time of 4 days (ref. 5). Observations indicate an increase in O_3 of 0.16 ± 0.05% for a 1% increase in 205-nm radiation, and a response time of 2 ± 1 days (ref. 5). Thus, the HNO_3 has an even stronger short-term response to solar ultraviolet variability than has ozone, and in the opposite sense.

It is difficult to study HNO_3 at higher altitudes because of the sharp decrease in concentration with altitude, but a similar study can be performed at 20 mbar over a smaller latitudinal interval (±20°) to minimize dynamical effects. Table 1 summarizes the results reported here and compares the model prediction (sensitivity (S) of HNO_3, expressed in per cent change, to a 1% increase in the solar 205-nm irradiance and the calculated time lag of the response) to the corresponding values derived from the LIMS data. The statistical analysis has been performed using the combined day and night data, the day data, and the night data, respectively. As the model provides 24-h averaged values, only the results provided by the combined day and night data should be compared with the calculated sensitivities. As expected, the correlation coefficient (r) is higher for the daytime observations than for the night-time. A solar effect is, nevertheless, still visible in the night data, because the signature of the daytime photochemistry is essentially frozen during the night and is degraded principally by dynamics. The theoretical sensitivities calculated for the 13.5- and 27-day periods are in good agreement at 10 mbar with the value obtained from the data analysis, but are smaller than the observation at 20 mbar. One should, however, recall that the model provides globally-averaged sensitivities, whereas the data used for the 20 mbar analysis proceed from observations confined to the tropics, where sensitivities should be higher.

Because the photodissociation of HNO_3 leads to the formation of nitrogen oxides, there should also be a solar effect on the NO_2 mixing ratio. The LIMS NO_2 data, averaged in the same way as the HNO_3 data, show a rapid response time (less than 1 day) and positive correlation with the solar irradiance. At 10 mbar, an increase in combined day and night NO_2 of 0.22 ± 0.12% is found, for a 1% increase in the 205-nm solar irradiance. The model[13,14] provides a corresponding increase of 0.15% in NO_2 for the 24-h average conditions. The observed NO_2 sensitivity on the dayside is larger ($+0.36 \pm 0.15$%).

The variation in the nitric acid concentration in the stratosphere over the 11-yr solar cycle can be estimated by calculating the HNO_3/ultraviolet sensitivity from a steady-state version of the model and by scaling the amplitude of the 205-nm solar forcing to the assumed 11-yr variation. If a 10 ± 5% increase is adopted for the 205-nm solar irradiance (based on a number of studies, including a regression analysis between detrended 205-nm and 10.7-cm solar irradiance over a period of 4 yr), the resulting long-term variation in the HNO_3 mixing ratio is estimated to be -10 ± 5% at 10 mbar and -5 ± 2% at 20 mbar. The sensitivity of the HNO_3 concentration to the solar ultraviolet irradiance is thus significantly increased for this longer-period oscillation. Such a large variation may be detectable in long-term measurements of HNO_3.

The detection of a solar signal in the LIMS HNO_3 and NO_2 variations provides a new test of the validity of currently assumed photochemistry in the stratosphere. Indeed, the HNO_3 response to short-term solar variability depends on several simultaneous photochemical processes, including the sensitivity of the HNO_3 photodissociation rate to the solar radiation near 200 nm and the sensitivity of HNO_3 production to variations in NO_2 and OH. These latter parameters are modulated through O_3 and N_2O variations caused by solar ultraviolet changes. The

Table 1 Response of HNO_3 to 205-nm solar variability

Pressure (mbar)	Model prediction 13.5 days	Model prediction 27 days	Combined day and night S	Combined day and night r	Day S	Day r	Night S	Night r	Δ lat.
10	−0.37	−0.42	-0.42 ± 0.07	−0.74	-0.44 ± 0.07	−0.78	-0.42 ± 0.12	−0.58	±40°
20	−0.13	−0.15	-0.29 ± 0.08	−0.57	-0.35 ± 0.09	−0.59	-0.25 ± 0.13	−0.34	±20°

Sensitivity, $S \equiv \dfrac{(HNO_3 - \overline{HNO_3})/\overline{HNO_3}}{(I_{205} - \bar{I}_{205})/\bar{I}_{205}}$; correlation coefficient, r. Time lag at both altitudes: 0.5 ± 0.5 days (model) and 0 ± 1.0 days (data analysis).

observed amplitude and phase of the responses at 10 mbar of HNO_3 and NO_2 to solar ultraviolet variability are in fair accord with predicted responses based on the currently accepted chemical scheme[18] used in the model. The results also imply large variations of HNO_3 over the 11-yr solar cycle, which should significantly affect other chemical species, including ozone. Indeed, increased solar activity can result in increased conversion of HNO_3 into active NO_x, which in turn can affect the ozone balance.

We thank J. M. Russell III for providing data on HNO_3, NO_2 and temperature from the Nimbus 7 LIMS experiment in November 1983, D. F. Heath for providing 205-nm solar spectral irradiance values from the Nimbus 7 SBUV experiment in August 1984, and J. E. Nealy for photochemical calculations. Some of this work was accomplished under NASA contract NAS1-15785 and CMA contract 83-468.

Received 18 February; accepted 11 March 1986.

1. Keating, G. M. *Sol. Phys.* **74,** 321-347 (1981).
2. Chandra, S. *J. geophys. Res.* **89,** 1373-1379 (1984).
3. Hood, L. L. *J. geophys. Res.* **89,** 9557-9568 (1984).
4. Gille, J. C., Smythe, C. M. & Heath, D. F. *Science* **225,** 315-317 (1984).
5. Keating, G. M., Brasseur, G. P., Nicholson III, J. Y. & De Rudder, A. *Geophys. Res. Lett.* **12,** 449-452 (1985).
6. Heath, D. F. & Schlesinger, B. M. in *Atmospheric Ozone* (eds Zerefos, C. S. & Ghazi, A.) (Reidel, Dordrecht, 1985).
7. Hood, L. L. *J. geophys. Res.* **91,** 5264-5276 (1986).
8. Chandra, S. *J. geophys. Res.* **91,** 2719-2734 (1986).
9. Gille, J. C. *et al. J. geophys. Res.* **89,** 5179-5190 (1984).
10. Russell III, J. M. *Adv. Space Res.* **4,** (4), 107-116 (1984).
11. Russell III, J. M. *et al. J. geophys. Res.* **89,** 5099-5107 (1984).
12. Heath, D. F., Donnelly, F. F. & Merrill, R. G. *NOAA tech. Rep.* No. ERL 424-ARL7 (1983).
13. Brasseur, G., De Rudder, A., Keating, G. M. & Pitts, M. *J. geophys. Res.* (submitted).
14. Brasseur, G., De Rudder, A. & Roucour, A. in *Proc. int. Conf. Environmental Pollution,* 839-910 (University of Thessalonika, 1982).
15. Brasseur, G. & Simon, P. C. *J. geophys. Res.* **86,** 7343-7362 (1981).
16. Biaumé, F. *J. Photochem.* **2,** 139-149 (1973).
17. Crutzen, P. & Schmailzl, U. *Planet. Space Sci.* **31,** 1009-1032 (1983).
18. Demore, W. B. *et al. Jet Propulsion Lab. Publ.* No. 85-37 (1985).

Novel experimental investigation of spontaneous ignition of gaseous hydrocarbons

J. F. Griffiths & W. Nimmo

Department of Physical Chemistry, The University, Leeds LS2 9JT, UK

Studies of spontaneous ignition of gases under rapid compression[1–3] are directed mainly towards understanding 'knock' in spark-ignition engines and the duration of ignition delays in diesels. The relevance to engine combustion lies in the ability to investigate the effects of fuel structure on the development of spontaneous ignition (arising either in different isomers of a hydrocarbon or due to reaction of mixtures of different hydrocarbons), while avoiding complicating practical features such as droplet evaporation, induction and exhaust of the charge, reciprocating piston motion and cycle-to-cycle variations. We report here a novel development, in which a variable-speed impeller in the combustion chamber of a rapid compression apparatus is used, first, to bring about spatial uniformity of temperature and concentration throughout the ignition delay period and, second, to enhance the rate of heat dissipation by successive increases in the speed of rotation. We show that, at given conditions for rapid compression, spontaneous ignition ceases to be possible beyond a limiting rotor speed.

The single-shot rapid compression machine[4] is operated at a compression ratio ($V_{initial}/V_{final}$) of 10.6:1 and at a combustion chamber temperature (T_a) of 293 K. During operation the piston travels 23.2 cm from its initial position in ~22 ms and on completion of its stroke has compressed the pre-loaded (33.0 kN m^{-2}), pre-mixed gaseous reactants into a squat cylindrical chamber of volume 31.9 cm^3 and depth 1.92 cm. End-of-compression pressures are ~0.9 MN m^{-2} (~9 atm) yielding, at the moment the piston stops, gas temperatures (T_c) of 775 K in the present study. A virtually ideal adiabatic compression is achieved, and so this temperature is determined by the relationship $T_c/T_a = (V_i/V_f)^{\gamma-1} = (P_f/P_i)^{\gamma-1/\gamma}$, where γ is the ratio of the principal specific heats of the reactant mixture. Our choice of initial composition, 0.03 nC_4H_{10} + 0.20 O_2 + 0.77 Ar, is governed by the desire to achieve the highest possible initial temperature, using the present mechanical system, in reactants that mimic 'typical' hydrocarbon-air mixtures in engines. Thus a stoichiometric proportion of fuel to oxygen is used, but the nitrogen is substituted by argon so as to augment γ as far as possible. The highest value for γ is that of the monatomic gases ($\gamma = 5/3$), but only in this limit is γ independent of temperature. In practice, for mixtures of gases, γ is derived at the compression temperature by an iterative procedure using a second-order polynomial representing the molar heat capacity as a function of temperature for each component of the system.

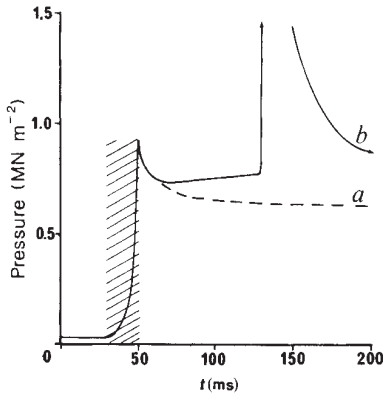

Fig. 1 Pressure-time records for non-reactive (*a*) and reactive (*b*) compositions compressed rapidly under identical conditions in the absence of mechanical stirring. Ignition occurs after a delay of 80 ms from the time when rapid piston motion ceases. The shaded area represents the interval during which rapid piston motion takes places. The zero of time is selected by the microcomputer control system.

Butane, in its isomeric *n*- and iso-forms, is the simplest hydrocarbon with which the effect of structural change on the spontaneous ignition behaviour of hydrocarbons can be investigated. Its gaseous state is preserved throughout the course of compression. This report concerns only *n*-butane.

Pressure changes that take place during compression, and afterwards in the closed, constant-volume chamber, are measured by a pressure transducer and recorded digitally. Because there is no significant loss of material by leakage and because the reactant is in sufficiently great dilution that only a very small change in the number of moles of material occurs during reaction, any pressure change measured during the post-compression period reflects a temperature change. Thus, in non-reactive compositions (Fig. 1, curve *a*) the gas temperature (and thus pressure) falls from its maximum at the end of piston travel due to heat loss to the walls. The pressure record can be used to calculate a mean gas temperature when heat transfer occurs only by residual gas motion due to the preceding piston motion. When vigorous mechanical stirring is introduced, the measured pressure is directly proportional to the spatially uniform gas temperature. Quantitative interpretations of heat release and dissipation rates may then follow[3].

Curve *b* in Fig. 1 is the pressure record obtained, in the absence of stirring, in a reactive composition of the same heat